

Review

Carlos Gutiérrez-Merino: Synergy of Theory and Experimentation in Biological Membrane Research

Silvia S. Antollini ¹  and Francisco J. Barrantes ^{2,*} 

¹ Departamento de Biología, Bioquímica y Farmacia, Universidad Nacional del Sur, Instituto de Investigaciones Bioquímicas de Bahía Blanca (CONICET-UNS), Bahía Blanca 8000, Argentina; silviant@criba.edu.ar

² Laboratory of Molecular Neurobiology, BIOMED UCA-CONICET, Buenos Aires C1107AAZ, Argentina

* Correspondence: francisco_barrantes@uca.edu.ar

Abstract: Professor Carlos Gutiérrez-Merino, a prominent scientist working in the complex realm of biological membranes, has made significant theoretical and experimental contributions to the field. Contemporaneous with the development of the fluid-mosaic model of Singer and Nicolson, the Förster resonance energy transfer (FRET) approach has become an invaluable tool for studying molecular interactions in membranes, providing structural insights on a scale of 1–10 nm and remaining important alongside evolving perspectives on membrane structures. In the last few decades, Gutiérrez-Merino's work has covered multiple facets in the field of FRET, with his contributions producing significant advances in quantitative membrane biology. His more recent experimental work expanded the ground concepts of FRET to high-resolution cell imaging. Commencing in the late 1980s, a series of collaborations between Gutiérrez-Merino and the authors involved research visits and joint investigations focused on the nicotinic acetylcholine receptor and its relation to membrane lipids, fostering a lasting friendship.

Keywords: Förster resonance energy transfer (FRET); membrane biophysics; membrane proteins; membrane lipids; lipid–protein interactions; nicotinic acetylcholine receptor



Citation: Antollini, S.S.; Barrantes, F.J. Carlos Gutiérrez-Merino: Synergy of Theory and Experimentation in Biological Membrane Research. *Molecules* **2024**, *29*, 820. <https://doi.org/10.3390/molecules29040820>

Academic Editors: Manuel Aureliano, Carmen Lopez-Sanchez and Alejandro Samhan-Arias

Received: 12 January 2024

Revised: 6 February 2024

Accepted: 7 February 2024

Published: 10 February 2024



Copyright: © 2024 by the authors. Licensee MDPI, Basel, Switzerland. This article is an open access article distributed under the terms and conditions of the Creative Commons Attribution (CC BY) license (<https://creativecommons.org/licenses/by/4.0/>).

1. Introduction

Professor Carlos Gutiérrez-Merino belongs to a group of curious and restless scientists who have contributed with incisive theoretical approaches and solid experimental work to the advancement of our knowledge in the highly complex and competitive field of biological membranes. He first approached us in the late 1980s, leading to a fruitful scientific collaboration entailing several research visits to carry out experimental work at the Institute for Biochemical Research of the Universidad Nacional del Sur in Bahía Blanca, Argentina, and reciprocated by visits of F.J.B. to Prof. Gutiérrez-Merino's laboratory at the Department of Biochemistry and Molecular Biology of the University of Extremadura in Spain, catalyzed by the Cooperation Programme with Iberoamerica. These exchanges extended throughout two decades, resulted in the publication of eight research papers, and helped forge a strong friendship with Carlos, a cultivated and warm-hearted individual who generously devoted many hours to teaching and holding discussions with research students and members of staff in our laboratory.

Biological membranes are complex and dynamic and remain the subject of multiple controversies. Various theories and models were suggested before Singer and Nicolson proposed the fluid-mosaic model in 1972 [1]. The innovative depiction of a biological membrane of the Singer and Nicolson model gained wide acceptance, provoking ample discussions, triggering experiments, and ultimately shedding light on membrane structure and function. The model has withstood the test of time, with various modifications and extensions, despite the enormous amount of new information gained during the last decades, some of which openly challenged the fluid-mosaic depiction [2–5].

Currently, a biological membrane is conceptualized as an intricate, crowded structure with a diverse lipid and protein composition, featuring lateral and transverse asymmetry, variable patchiness, variable thickness, and high protein occupancy [2,5]. It is universally accepted that biological membranes act as barriers that separate two fluid media, preventing direct contact between the inner and outer compartments. However, constituting a physical barrier is not their sole function. Many essential biochemical reactions for cell life, involving metabolic and signaling processes with membrane-bound enzymes and transmembrane proteins such as G-protein coupled receptors (e.g., rhodopsin or muscarinic receptors) and ion channels (e.g., nicotinic, histaminergic, GABAergic, or glutamatergic receptors), take place in cell membranes. This makes membranes pivotal scenarios in nearly all cellular physiological and pathological processes. These essential reactions require molecular communication, involving both protein–protein and protein–lipid interactions, and the study of these processes posed formidable experimental challenges a few decades ago.

2. Gutiérrez-Merino's Development of Theoretical Approaches in Fluorescence Spectroscopy in Biological Membrane Research

At the time when the fluid-mosaic membrane model was being developed, Förster resonance energy transfer (FRET) emerged as a revolutionary and extremely useful technique for the study of molecular interactions in biological systems, as it allows the obtention of structural details in the 1–10 nm scale size [6–8]. FRET theoretical developments addressing the analysis of experimental data permitted biophysicists to extract quantitative information about a great variety of membrane properties [9–26].

One of Gutiérrez-Merino's contributions to the field of FRET took the form of two theoretical approaches that were presented almost simultaneously. One of these approaches was developed for model systems of binary lipid mixtures undergoing phase separation and involving four main conditions: (a) a triangular network of lipids in a gel phase [27]; (b) an insignificant relative population of small clusters; (c) donor and acceptor molecules oriented in the plane of the membrane (achieved at very low concentrations of labeled lipids, typically <5%); and (d) a substantial number of acceptor molecules for each donor molecule [17]. The acceptor molecules were assumed to be situated in concentric layers of lipid (discs) around a single donor molecule.

The rate of energy transfer (k_T) between a donor and an acceptor separated by a distance r was calculated using the value of $K_T(r)$ obtained with Förster's equation [28], and the relative number of phospholipid molecules in each disc with respect to the number of phospholipid molecules in the first disc around a given molecule (Equation (1)) was formulated as follows:

$$k_T(r) = \tau_0^{-1} (R_0/r)^{-6} \quad \text{with } k_T = [k_T(r)/k_T(r_1)] n/6 \quad (1)$$

where τ_0 is the lifetime of the donor in the absence of the acceptor; R_0 is the distance in Å between donor and acceptor molecules at which the transfer efficiency is 50%; r_1 is the average intermolecular distance of the triangular lattice; and n is the number of phospholipid molecules in each disc surrounding a given phospholipid molecule. Considering the random distribution of donor and acceptor molecules in the plane of the membrane, it is assumed that no change takes place in the orientation factor κ^2 (a parameter used in the calculation of R_0) in the passage from one lipid disc to the next [17].

Considering the rate of energy transfer, theoretical analyses were developed for a binary, partially mixed lipid bilayer undergoing lateral phase separation (Equation (6)), intended to represent a realistic condition met in biomembranes [17]. The root of this reasoning stems from the analysis of both an ideal mixture of lipids (Equation (2)) and a completely immiscible mixture of lipids (Equations (3) and (4)). In both cases, the experimental data were obtained from unilamellar vesicles, whereby the bilayer curvature was considered negligible.

$$k_T = [1 - N_A/(N_A + N_B)] f_a k_T(r_1) \quad (2)$$

where N_A and N_B are the number of molecules of randomly distributed donor and acceptor lipids, respectively, and f_a is the fraction of B molecules.

$$k_T = [(2n + 6)/6n] f_a k_T(r_1) \quad (3)$$

where n is the number of lipid molecules in a cluster consisting of up to six molecules of the minority component in the lipid mixture, with completely immiscible A and B molecules, and

$$k_T = (6n)^{-1} \{6 + 12 [s + n_{exc}/6 (s + 1)]\} f_a k_T(r_1) \quad (4)$$

where s is the number of complete lipid shells of the cluster, which is an integer ≥ 1 , and n_{exc} is the number of lipid molecules in the incomplete outer shell of the cluster.

Next, the rate of energy transfer for a binary partially mixed lipid bilayer undergoing lateral phase separation is calculated, as follows:

$$k_T = f_a k_T(r_1) \langle i \rangle^{-1} (\langle 1/i \rangle + 2\langle s_i/i \rangle) \quad (5)$$

where i corresponds to lipid molecules of class A, and $\langle i \rangle$ and $\langle s_i/i \rangle$ are the average cluster size in terms of number of lipid molecules within and the ratio of cluster shells to lipid molecules in the cluster, respectively. Equation (5) can be reformulated by expressing the last term as $\langle (1 + 2s_i)/i \rangle = \frac{1}{2} \langle D_i/i \rangle$, where D_i is the diameter of the circular cluster i , and $\langle D_i/i \rangle = \langle D_i - 1 \rangle$. Thus,

$$k_T = \frac{1}{2} f_a k_T(r_1) \langle i \rangle^{-1} \langle D_i^{-1} \rangle \quad (6)$$

This allows one to calculate the average cluster size of the minority lipid (lipid A).

In summary, the average energy transfer efficiency provides a means to ascertain, directly from experimental observations, the average size of lipid clusters, correlating this information with the concentrations of both lipids in the mixture, within constrained molar fraction ranges. These novel contributions from Gutiérrez-Merino significantly contributed to enhancing our understanding of the thermodynamic principles governing lateral phase separation in lipid membranes [17].

The scope of this analysis was broadened to encompass additional conditions, in particular the inclusion of membrane proteins, as addressed in the second theoretical approach based on FRET, which Gutiérrez-Merino introduced more than forty years ago [18]. In this scenario, the assumption (a) of the first approach required modifications to incorporate the distribution and state of aggregation of integral membrane proteins. Again, FRET experiments conducted on these more complex biological systems were key to reaching the conclusion that the average rate of energy transfer could function as a quantitative ruler of the following, among other metrics of membrane properties: (a) transmembrane distances (i) between proteins or (ii) between proteins and lipids; (b) distances between sites within a single protein; (c) changes in protein aggregation; (d) lipid heterogeneities; and (e) random or non-random protein distribution. Measurements of the average rate of energy transfer between protein and phospholipid molecules, labeled with donor and acceptor molecules, respectively, were often used in these experiments. The ability to accurately characterize the above properties and processes strongly depends on the careful selection of donor and acceptor molecules. For example, in the examination of random and non-random protein distributions in a membrane, it is imperative to employ fluorescently labeled proteins for the donor-acceptor pair. To investigate protein lateral phase separation from lipids, it is usually necessary to resort to a donor-labeled protein and acceptor-labeled lipids. In the latter case, it is crucial to verify that the fluorescent label of the lipids does not exclude them from the immediate perimeter of the protein or induce non-preferential binding to the protein of interest [18].

The above theoretical approach was applied to the study of the $(Ca^{2+}-Mg^{2+})$ ATPase. In this case, ATPase labeled with a fluorescein tag at the ATP binding site served as the donor, and rhodamine-labeled lipids acted as acceptors. This configuration allowed the fluorescently labeled ATP binding site of the enzyme to sit at a distance from the lipid-

water interface of the membrane. Moreover, this series of experiments made it possible to postulate that the $(\text{Ca}^{2+}\text{-Mg}^{2+})$ ATPase existed as a dimer, with the ATP binding sites of each monomer located close to the protein–protein interface [29]. Subsequently, using Co^{2+} as an acceptor for the fluorescence emitted by fluorescein and employing the same theoretical approach, it was possible to establish the location of functional binding sites, in particular the regulatory metal ion sites for free Co^{2+} , which likely correlate with Ca^{2+} sites (Figure 1A) [30].

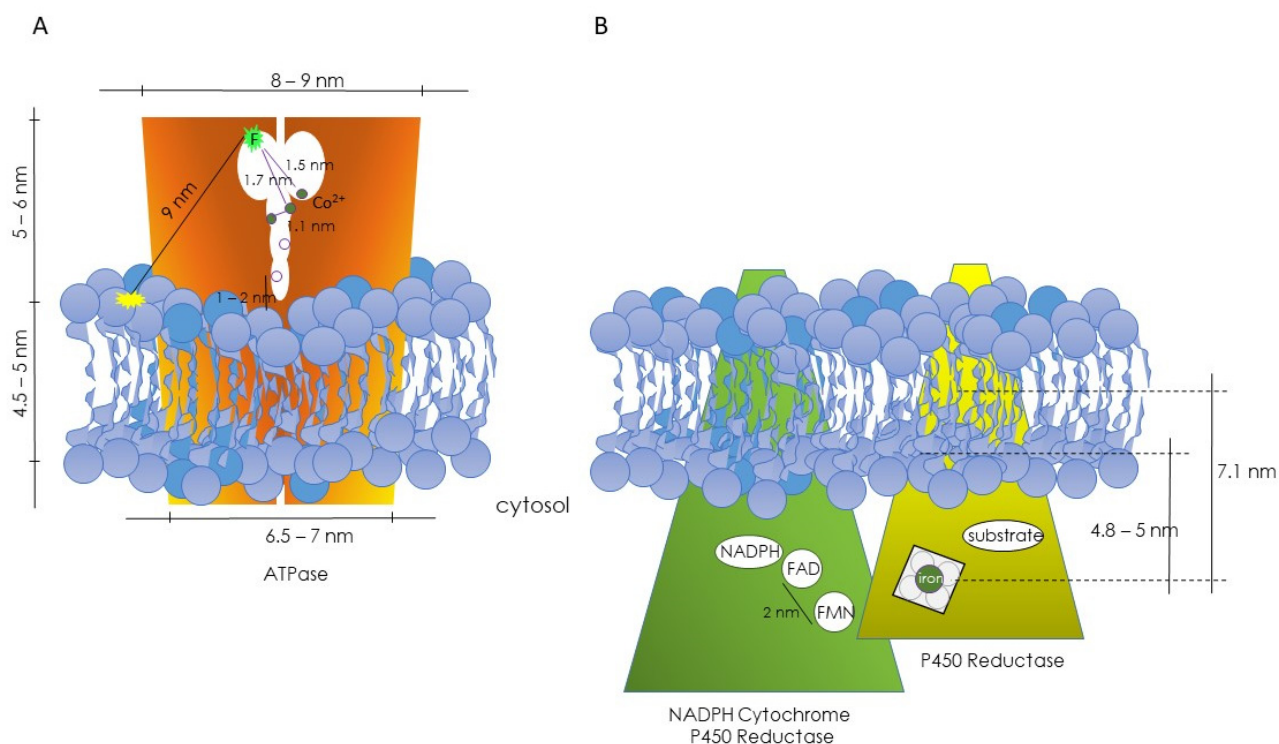


Figure 1. Diagrams depicting the hypothetical topographical relationships between the ATPase (A) and NADPH cytochrome P450 reductase and P450 reductase (B) with their respective lipid microenvironments. In both cases, information was obtained through FRET studies. (A) From Gutiérrez-Merino et al., refs. [29,30]. (B) From Centeno and Gutiérrez-Merino, ref. [31].

In 1994, Gutiérrez-Merino and colleagues [32] extensively discussed the utilization of FRET for measuring distances between donor and acceptor molecules, building upon their prior expertise [29–31,33]. As is now well established, this nonradiative process involves the transfer of excitation energy through long-range dipole–dipole coupling, a phenomenon affected by the distance between the two molecules and their orientation [28]. A significant cautionary note was issued regarding the precision of such measurements. Obtaining a single donor–acceptor pair in membrane systems is challenging unless very restrictive conditions are met, such as an R_0 value smaller than half the dimension of the protein diameter or a homogeneous dispersion of monomeric membrane proteins with substantial “dilution” in a lipid matrix. Hence, calculations of distances between two functional protein sites or a protein site and a lipid pose considerable uncertainty.

A similar reasoning was employed to investigate the positioning of functional centers in the microsomal cytochrome P450 system [31]. Energy-transfer studies enabled the determination of the locations of the two prosthetic groups (FAD and FMN) of NADPH-cytochrome P450 reductase, as well as the heme group and the substrate binding site of cytochrome P450 (Figure 1B). The estimated distance between the FAD and FMN groups (donor–acceptor pair) was approximately 2 nm. Using a lipid labeled with rhodamine (RPE) as an acceptor for the reductase’s fluorescence, the position of the flavins was estimated

to be more than 5 nm from the rhodamine group. Consequently, it was concluded that the FMN and FAD groups are not exposed to the enzyme's surface and are distant from the lipid–water interface, with FAD more deeply buried than FMN in the enzyme's 3D structure. In the case of cytochrome P450, two different donor–acceptor pairs were used: diphenylhexatriene (DPH)–heme and 4H7HC–heme, with DPH located deep inside the lipid bilayer, and the coumarin group of 4H7HC close to the polar headgroup. Distances of 7.1 nm between the heme and DPH groups and of approximately 4.8 nm from the heme group to the lipid–water interface were obtained. A third donor–acceptor pair was used (ethoxycoumarin–heme group). Ethoxycoumarin is a good substrate for these isoenzymes, and a distance of 5.3 nm between the heme group and 7-ethoxycoumarin could be calculated (Figure 1B) [31].

3. Gutiérrez-Merino's Incursions into the Field of Nicotinic Acetylcholine Receptor–Lipid Interactions

The influence of lipids on the conformation, function, and topography in the membrane of the nicotinic acetylcholine receptor (nAChR) has been the subject of intense study for the last 50 years [34]. Synthesis, assembly, and function of the nAChR strongly depend on the properties and characteristics of the membrane in which it is embedded. The layer of lipids in the immediate vicinity of the receptor has distinct properties relative to bulk lipids. Different experimental strategies have been used over the last decades to investigate receptor–lipid interactions. Fluorescence spectroscopy and fluorescence microscopy have occupied a central position in characterizing many of the properties of the nAChR that we now know of. Carlos Gutiérrez-Merino contributed to this endeavor during his collaboration with our laboratory in the early 1990s. In this Section, we will summarize some of these studies.

nAChRs are pentameric integral membrane proteins belonging to the Cys-loop superfamily of ligand-gated ion channels [35–38]. Each of its five subunits possesses a large extracellular region that harbors the agonist-binding site, a transmembrane region with extensive contacts with surrounding lipids through evolutionarily conserved structural motifs [34,39–41] and an intracellular region containing modulatory sites and determinants of channel conductance [42,43]. The transmembrane domain consists of four segments (TM1–TM4), with TM2 forming the walls of the ion channel pore and TM1, TM3, and TM4 being more externally located [34,44,45]. Among these, TM4, the most peripheral transmembrane domain, has the closest contact with membrane lipids and constitutes the lipid-sensing domain of the protein [46,47].

The nAChR is a typical transmembrane protein, and the properties and characteristics of the membrane in which it resides are therefore important influences on its function, biosynthesis, and proper assembly [36,46–50]. Reciprocally, the nAChR exerts influence on its neighboring lipids [51–53]. The muscle-type nAChR at the neuromuscular junction and the electric fish of electromotor synapses (electric eels and electric rays) is enveloped by a layer of interstitial lipids, relatively immobilized in the microsecond time-window of electron spin resonance (ESR) spectroscopy, with distinct features relative to bulk lipids [51]. Thus, the lipid molecules closely associated with the protein exhibit a slow exchange rate with bulk lipids. Mobile lipids interact with membrane proteins in a relatively less specific manner and exhibit a faster rate of exchange with bulk lipids [54–57]. It has been stressed that in contrast to other biological membranes, the postsynaptic membrane in which the nAChR is embedded is a unique system, whereby the amount of bulk lipid in the tight 2-dimensional lattice of receptor proteins is minimal, with only a few layers of interstitial lipid in between adjacent receptor molecules, and consequently with little, if any, “bulk” lipid [34].

Since lipid composition undergoes changes with aging and in response to various neurodegenerative diseases [58,59], and bearing in mind that lipid content varies across different tissues, it becomes imperative to comprehend how alterations in the nAChR lipid environment impact its structure, activity, and dysfunction.

One key aspect of biological membranes is their heterogeneity, which comprises both lateral and transbilayer asymmetries, two topographical properties that have an impact on integral membrane proteins. The aminophospholipids phosphatidylethanolamine (PE) and phosphatidylserine (PS), along with phosphatidylinositol, are primarily situated in the inner leaflet of the plasmalemma, while phosphatidylcholine (PC) and sphingomyelin (SM) are predominantly located in the outer leaflet in most mammalian cells [60,61]. In mouse synaptic plasma membranes, the outer monolayer exhibits greater fluidity than the inner leaflet [62,63], a phenomenon that correlates with the notable prevalence (88%) of cholesterol in the inner, cytoplasmic hemilayer in some biological membranes [64]. In one of Gutiérrez-Merino's visits to our laboratory, we explored lipid asymmetry in native nAChR-rich membranes from *Torpedo* electrocytes. The dimensions of a lipid bilayer, typically ranging from 4 to 5 nm [65,66], fall within the same range as the R_0 observed between different pairs of donor and acceptor fluorescent molecules commonly employed in biophysical studies of biological membranes. Hence, it was predicted that the efficiency of FRET between lipids labeled as donor and acceptor in opposite leaflets of the membrane bilayer would be significantly lower than the transfer between donor and acceptor molecules located on the same membrane hemilayer. We used lipids tagged with an NBD group as donor, labeled at various positions such as the headgroup, C6, and C12. The fluorescent probe rhodamine-PE (N-Rho-PE) was chosen as the acceptor. A calculated R_0 value of 5.58 nm for the donor–acceptor pair was determined [67]. We concluded that the phospholipids PC and PE were primarily located in the exofacial leaflet in nAChR-enriched membranes from *Torpedo*. Additionally, the evaluation of energy transfer efficiency reported deviations from a uniform distribution of the labelled lipids within this leaflet when high molar ratios of acceptor lipids were used in liposomes prepared with the endogenous PC fraction extracted from native nAChR-rich membrane samples.

In a subsequent study, we addressed the precise location of SM in native nAChR-rich membranes from *Torpedo marmorata*. At that time, the distribution of SM on the cell-surface membrane was not known, nor was it clear whether this lipid held any structural and/or functional significance relative to the major functional molecule in this membrane, the nAChR. Previous work had shown the enrichment of SM in membrane regions where nAChR clusters were present. The lipid composition of these regions differed from the bulk membrane composition [68]. In nAChR-rich membranes derived from the electric organ of Torpedinidae species, the primary phospholipids were PC (40%), PE (35%), and PS (13%), with a much lower SM content (~5% of the total phospholipid content) [69,70]. Using classical biochemical approaches, it was possible to conclude that SM in native nAChR-rich membranes from *T. marmorata* was enriched in the outer membrane hemilayer, confirming the transbilayer asymmetry of this lipid. However, this did not imply homogeneity in the distribution of SM in the external hemilayer. To address this question, N-[10-(1-pyrenyl)decanoyl] sphingomyelin (Py-SM) was used as a reporter group of the lipid physical state. FRET was also employed to assess the spatial relationship between the receptor protein and the fluorescent lipid analogue in the immediate vicinity of the nAChR protein as well as to determine its affinity for the receptor.

The ratio of excited-state pyrene dimer (excimer) to monomer Py-SM fluorescence (FE–FM) provides insight into the intermolecular collisional frequency of these fluorophores; hence, it constitutes a parameter directly affected by probe concentration. The increased rate in the FE–FM ratio as a function of Py-SM concentration was twofold higher under FRET conditions than under direct excitation of the probe. This observation suggested a preferential partitioning of the Py-SM analogue in the protein-adjacent region. Applying one of Gutiérrez-Merino's theoretical FRET approaches [17,18] to the experimental data enabled us to determine R_0 . A value of $21 \pm 2 \text{ \AA}$ was obtained, in good agreement

with previous reports [71]. The new data permitted the calculation of the k_r for SM in the nAChR vicinity; a value of 0.55 relative to the average bulk lipid moiety in the membrane was obtained. This result suggested that Py-SM displayed a moderate affinity for the membrane-bound nAChR. Treatment of the membrane with sphingomyelinase converts SM into phosphorylcholine and ceramide (Cer). In intact membranes, enzymatic hydrolysis removes only outer leaflet SMs [72]. When nAChR-rich membranes were treated with sphingomyelinase and FRET efficiency was measured before and after enzymatic hydrolysis, a noticeable increase in FRET efficiency between the protein and the resulting Py-Cer was observed, indicating an enhanced affinity of Py-Cer for the donor protein and/or greater accessibility of this lipid to the lipid microenvironment of the nAChR relative to the Py-SM precursor. Additionally, a gradual decrease in the FE-FM ratio was observed during enzymatic digestion, reinforcing the idea that Py-Cer exhibits higher affinity and/or greater accessibility to the lipid-protein interface than Py-SM. This finding could be rationalized in terms of the structural similarity between Cer and free fatty acids (FFAs), since the latter exhibit approximately four times greater affinity for the membrane-bound *Torpedo* nAChR relative to PC [73,74]. Considering a total of 44 lipids comprising the nAChR vicinal lipid, only 2.2 molecules of SM were estimated to be at the nAChR-lipid interface [75]. If one considers that the conversion of SM to Cer, a process that occurs naturally and has significant functional consequences, could produce an increase in Cer molecules at the nAChR-lipid interface, it also implies a relative decrease in other lipids in the receptor microenvironment. These changes in the lipid-nAChR interface might entail functional consequences, given the well-known influence of lipids on the conformation and allosteric mechanisms of this receptor [34].

To learn about the physical characteristics of the membrane in which the nAChR is inserted and of the lipid belt region, we resorted to the amphiphilic fluorescent probe Laurdan (6-dodecanoyl-2-dimethylaminonaphthalene) [76]. Laurdan, one of the several solvatochromic probes conceived and synthesized by Gregorio Weber and colleagues, possesses an exquisite spectral sensitivity to the phase state of the membrane because of its capacity to sense the polarity and the molecular dynamics of dipoles in its surroundings, due to the effect of dipolar relaxation processes [77–79]. Laurdan localizes at the hydrophilic-hydrophobic interface of the lipid bilayer [80,81], with its lauric acid moiety at the phospholipid acyl chain region and its naphthalene moiety at the level of the phospholipid glycerol backbone. The so-called general polarization (GP) of Laurdan, a ratiometric fluorescence technique, exploits its advantageous spectral properties, as it was initially developed for time-resolved fluorescence emission spectral analysis in cuvette studies [76].

To learn about the physical state of the lipid microenvironment of the nAChR, we conceived a novel approach in Laurdan studies that relied on exploiting the Förster energy transfer from the intrinsic fluorescence of the nAChR (donor) to Laurdan as the acceptor, thus introducing FRET-GP in membrane biophysics [52]. As shown in Figure 2, the nAChR has 52 tryptophan residues, 51 at the transmembrane region and 1 at the extracellular domain. Using the structural data available at that time [82], we reasoned that the transmembrane Trp residues were arranged as an interconnected network in a ring-like three-dimensional structure with an outer radius of 32.5 Å. Furthermore, in view of the long-axis dimensions of the nAChR molecule and the width of the lipid bilayer [82], the height of the plane of nAChR tryptophan residues was allowed to vary between 0 and 50 Å (Figure 2). The nAChR cylinder was in turn assumed to be surrounded by a belt of lipid molecules of approximately 10 Å diameter each. The plane of acceptors was calculated assuming an area per lipid molecule of 0.75 nm² [83].

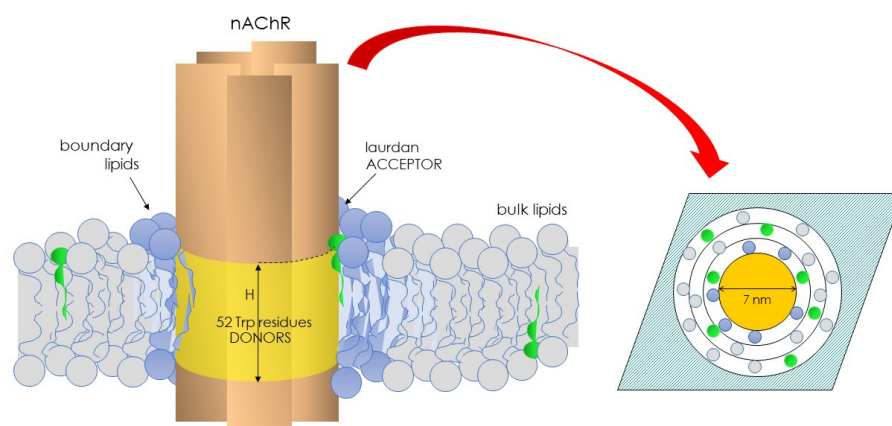


Figure 2. Illustration depicting the nAChR and its 52 Trp residues and the vicinal, boundary lipid of the Laurdan molecules' (green) partition. nAChR Trp residues act as donors, and the solvatochromic Laurdan molecules as acceptors. This pair constitutes the basis of the FRET-GP concept introduced in the field of biological membranes in 1996 (ref. [52]).

The parameter H was used as a measure of the distance between donor–acceptor planes normal to the membrane surface. Several conditions were considered [29]: (i) neighboring nAChR molecules did not generate an accessible surface area to acceptor molecules; (ii) the homotransfer of energy was allowed to occur between Trp residues; and (iii) a distance of closest approach (r) of 10 Å corresponding to the sum of the van der Waal radii of Trp and Laurdan was considered. The distribution (random or nonrandom) of Laurdan in the nAChR-vicinal lipid was calculated using the parameter α (Equation (7)), which considers the probability of occupancy of sites at the lipid belt region by Laurdan (L1) relative to unlabeled lipids (L2), as follows:

$$\alpha = (x_1/K_1)/(x_2/K_2) = (x_1/x_2) K_r^{-1} \quad (7)$$

where $x_1 + x_2 = 1$, and K_r is the apparent dissociation constant of Laurdan for the lipid belt region. A value of $K_r = 1$ implies random distribution of the probe in the membrane, whereas values less than or greater than 1 imply Laurdan's preferential partition at the lipid belt region or Laurdan's exclusion from this region, respectively. Theoretical fittings with varying R_0 , r , and H were performed and compared with the experimental data using a set of curves with different K_r values (from 0.01 to 100) with a fixed R_0 (Figure 3) [52]. An R_0 value of 29 ± 1 Å for an intrinsic fluorescence protein–Laurdan donor–acceptor pair was calculated. With this value, an average value of $r = 14 + 1$ Å was chosen for H between 0 and 10 Å (Figure 3A,B). This value corresponds to the thickness of a single layer of phospholipid molecules (0.75 nm^2 in surface area; [83]), in agreement with the proposed location of Laurdan in the bilayer [78,80,81]. Finally, a value of K_r near 1 was obtained (Figure 3C), indicating a random distribution of Laurdan in the lipid bilayer, confirming previous observations that suggested that the location of Laurdan in the membrane was independent of the nature of the phospholipid polar headgroup [78].

In practice, theoretical and experimental FRET efficiency (E) are related as follows:

$$E = k_T/k_0 + k_T = 1 - \phi/\phi_D \approx 1 - I/I_D \quad (8)$$

where k_0 is the rate of energy transfer, and donor and acceptor molecules are separated by R_0 ; ϕ and ϕ_D are fluorescence quantum yields of the donor in the presence and absence of acceptor molecules, respectively; and I and I_D are the fluorescence emission intensity of the donor in the presence and absence of acceptor molecules, respectively.

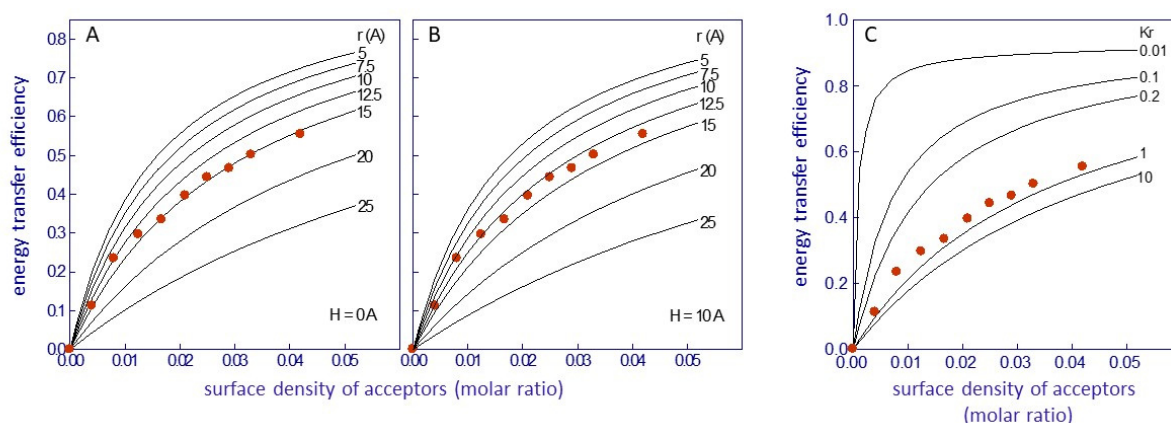


Figure 3. Efficacy of Förster resonance energy transfer (FRET) between the protein intrinsic fluorescence (nAChR) and Laurdan as a function of the surface density of energy transfer acceptors, in nAChR-rich membranes from *T. marmorata*. The continuous lines correspond to theoretical curves representing (A,B) minimal distances (r) between donor and acceptor, calculated utilizing the methodology proposed by Gutierrez-Merino [18], with $R_0 = 29 \text{ \AA}$ and H set at 0 \AA and 10 \AA , respectively, and (C) different values of the apparent dissociation constant of Laurdan for the boundary lipids (K_r), calculated using the treatment of Gutiérrez-Merino et al. [29], with $H = 0 \text{ \AA}$, $r = 15 \text{ \AA}$, and $R_0 = 29 \text{ \AA}$. Data taken from ref. [52].

The knowledge gained through these studies on the precise localization of Laurdan at the first shell of lipids surrounding the nAChR and the observation that the convenient positioning of Laurdan made it possible to use this probe as an acceptor of the nAChR intrinsic fluorescence in FRET-GP prompted us to undertake a series of studies on nAChR–lipid interactions in native membranes. Using fluorescence spectroscopy, we could identify sites for free fatty acids, various sterols, and phospholipids in the nAChR [84]. These sites were found to be preserved after controlled proteolysis of the extracellular nAChR moiety and were masked during nAChR desensitization [53]. Additionally, we utilized this fluorescent donor–acceptor pair to study nAChR localization in liquid-ordered and/or liquid-disordered domains in membranes of various compositions and asymmetries [85,86].

4. Gutiérrez-Merino’s Use of FRET in Imaging Studies of Biological Membranes

One of the most interesting aspects of FRET studies in membranes is the spatial selectivity, permitting the observation of phenomena restricted only to acceptor molecules that are just a few nanometers away from the donor molecule, thus providing high spatial resolution for the case of multiple acceptors per donor, a property that has been exploited in cell imaging.

Neuronal apoptosis is intimately related to oxidative stress [87], and a considerable amount of research has been undertaken in this field to understand not only physiological apoptosis but also that associated with pathophysiological conditions such as neurodegenerative diseases (i.e., Alzheimer disease [88]). Gutiérrez-Merino expanded the potential of FRET approaches by transitioning from cuvettes to the microscope, focusing on this challenging problem. Changes in the red/orange autofluorescence of flavoprotein cytochrome b5 reductase (Cb5R), a major component of the plasma membrane redox chain, and other flavoprotein oxidases also bound to membranes were observed under cellular oxidative stress conditions [89]. Thus, flavins were used as donor molecules to study their location in the plasma membrane. Two suitable acceptor molecules were *N*-(3-triethylammoniumpropyl)-4-(4-(4-(diethylamino)phenyl)butadienyl)-pyridinium dibromide (RH-414) and *N*-(3-triethylammoniumpropyl)-4-(6-(4-(diethylamino)phenyl)hexatrienyl) pyridinium dibromide (FM4-64), with the fluorescence of RH-414 homogeneously distributed in the plasma membrane [90], while FM4-64’s fluorescence is concentrated in the actively recycling membrane at synaptic connections [91]. At cerebellar granule neurons (CGNs), R_0

values for both pairs of donor–acceptor molecules were in the range of 3.7–4.2 nm, with a FRET efficiency of 30–35% at 9 days of cell culture (mature CGN). Fluorescence microscopy images of CGN stained with FM4-64 obtained at the donor wavelength excitation showed that FM4-64 is distributed in clusters or discrete membrane domains 0.5–1 μm in diameter, largely present at inter-neuronal contact sites of the neuronal soma [92].

The membrane-bound isoform of Cb5R is a major protein component of the plasma membrane redox chain in rat liver cells [93], one of the five more abundant proteins of the caveolin–protein complex isolated from the vascular endothelial membrane [94], and a flavoprotein. Thus, working with CGN, FRET studies were conducted between CTB-Alexa488 and anti-caveolin-2/IgG-Alexa488 (as lipid raft markers) and anti-Cb5R/IgG-Cy3. The observed FRET between CTB-Alexa488 and anti-Cb5R/Cy3 indicates that Cb5R must be present in most “lipid raft” domains of the plasma [95]. More recently, FRET imaging with cerebellar cortex slices using Alexa488-cholera toxin B as the donor and the complex anti-Cb5R isoform 3/IgG-Cy3 as the acceptor confirms that a large part of Cb5R isoform 3 is located vicinal to lipid raft nanodomains [96]. Further FRET studies using CGNs in culture, with a methodological improvement based on the implementation of secondary fluorescent antibodies (Alexa488-IgG and Cy3-IgG) directed against primary antibodies for Cb5R and L-type calcium channels (L-VOCC), led to the suggestion that L-VOCC was anchored to raft domains through binding to caveolin complexes. This could occur at a distance between 10 and 100 nm from cytochrome b5 reductase [97]. Similar FRET experiments showed an enhanced clustering of cytochrome b5 reductase within caveolin-rich lipid raft microdomains in the early phase of apoptosis [98]. A contemporary study using a great variety of donor–acceptor pairs indicated that (a) L-VOCC and N-methyl D-aspartate receptors (NMDARs) are vicinal proteins in the plasma membrane, separated by less than 80 nm; (b) NMDARs also colocalize with neuronal nitric-oxide synthase (nNOS); (c) nNOS is closer to caveolin-2 than caveolin-1; and (d) CTB binding sites were located extracellularly and nNOS sites intracellularly. Together, these findings suggested the clustering of NMDARs, L-VOCC, and nNOS in caveolin-rich microdomains with dimensions <100 nm. Gutiérrez-Merino and colleagues named these domains “calcium-microchip-like structures” and speculated that they have a high degree of control over the neuronal excitability by calcium [99]. The donor–acceptor pairs used were anti-L-VOCC/IgG-Alexa488 and anti-NMDAR/IgG-Cy3; anti-NMDAR/IgG-Alexa488 and L-VOCC ligand ST-BODIPY dihydropyridine, a much smaller molecule; anti-nNOS/IgG-Alexa488 and anti-NMDAR/IgG-Cy3; and anti-nNOS/IgG-Alexa488 and CTB-Alexa555 as donors and anti-caveolin-1/IgG-Cy3 and anti-caveolin-2/IgG-Cy3 as acceptors [99].

Additionally, co-localization of the calcium extrusion systems (PMCA, plasma membrane calcium pump, and NCX, sodium–calcium exchanger) with the major calcium entry systems (L-VOCC and NMDAR) and the ROS/RNS enzymes (Cb5R and nNOS) was observed within lipid raft-associated sub-microdomains smaller than 200 nm [100]. From these studies, lipid rafts emerged as interesting markers of plasma membrane nanodomains, where cross-talk between redox and calcium signaling occurs.

Recently, and as a continuation of the same approach, Gutiérrez-Merino and colleagues initiated a series of studies on Alzheimer’s disease, exploring the relationship between A β peptides, membrane lipids, and dysregulation of calcium homeostasis. FRET imaging was performed in mature CGN between the fluorescent derivative A β (1–42)-HiLyteTM Fluor555 and anti-CaM (calmodulin) conjugated with IgG-Alexa 488 (anti-CaM* A488) or anti-LTCC subunit 1C conjugated with IgG-Alexa 488 (anti-LTCCs* A488), and between anti-CaM* A488 and anti-HRas* Cy3. Several protein markers of lipid rafts were used as acceptors: anti-Cav-1 conjugated with IgG-Alexa 488 (anti-Cav1* A488), anti-HRas conjugated with IgG-Alexa 488 (anti-HRas* A488), and anti-PrPc conjugated with IgG-Alexa488 (anti-PrPc* A488). An extensive complexation of A β with CaM and LTCC with colocalization of CaM and HRas together with an A β association with lipid raft sub-microdomains was observed [101]. The dysregulation of calcium homeostasis observed in Alzheimer’s disease was attributed to the inhibition of LTCC by CaM–A β complexes.

In a subsequent study, using the same fluorescence-labeled A β and Alexa488-labeled secondary antibodies for primary anti-PDI and anti-CaM or stromal interaction molecule 1 (STIM1) labeled with green fluorescent protein (STIM1-GFP), Gutiérrez-Merino and colleagues demonstrated that prior to the internal dysregulation of calcium homeostasis, a perturbation of store-operated calcium entry occurs through the internalization of A β and its inhibition of STIM1, along with partial activation of the ER Ca²⁺-leak channels [102]. For these measurements, variations in donor fluorescence were analyzed, and the R_0 and the spectral overlap integral (J) values were obtained for the A β *555–SPM1-GFP donor–acceptor pair [102]. Recently, based on a similar formalism, Gutiérrez-Merino and colleagues showed that a short peptide of only six histidines binds with high affinity to A β (1–42) and also to A β (25–35), which still remains toxic, blocking the interaction of A β with CaM and calbindin-D28k [103]. This latest result opened an interesting line of research on the modulation of A β peptide toxicity.

5. Concluding Remarks and Future Prospects

In his “Zwischenmolekulare Energiewanderung und Fluoreszenz (Intermolecular energy migration and fluorescence)” [28] and “Experimentelle und theoretische Untersuchung des zwischenmolekularen Übergangs von Elektronenanregungsenergie” [104] papers, Theodor Förster set the theoretical basis of what we currently know as the Förster resonance energy transfer (FRET) phenomenon, a non-radiative process through which a donor fluorophore in the excited state transfers energy to nearby acceptor molecules within nanometric distances. Lubert Stryer and Richard Haugland were among the first to qualify FRET as a “spectroscopic ruler” [105]. Gregorio Weber, another forefather of fluorescence spectroscopy in biological applications, considered FRET as the ultimate yardstick in intermolecular and intra-molecular measurements in solution. Carlos Gutiérrez-Merino made ample use of FRET in his many studies on biological systems and contributed to setting the theoretical basis for the application of FRET in biological membrane research. During our decade-long collaboration with Carlos Gutiérrez-Merino, we conceived the use of FRET in combination with the so-called general polarization of Laurdan, a solvatochromic fluorescent probe designed and synthesized by Gregorio Weber [106]. This combination resulted in FRET-GP, the first application of Laurdan as a sensor of a membrane-embedded protein’s lipid microenvironment by excitation of the protein’s intrinsic fluorophores [52].

The emergence of autofluorescent proteins and protein chimeras with spectroscopic characteristics suitable for FRET applications has opened the way to implement Förster resonance energy transfer in the light microscope. The study of four-dimensional (x,y,z,t) molecular-scale phenomena in live cells [107] is thus a reality that now projects beyond the optical diffraction barrier and into the realm of super-resolution light microscopy [108–114]. Furthermore, the ability to genetically manipulate the chemistry of donor and acceptor fluorescent proteins has expanded the spectral coverage of fluorescence microscopy in live-cell interrogation [110]. These advances are particularly relevant to the field of membrane biology. Hybrid FRET models that incorporate fluorescence spectroscopy concepts, optical microscopies, and artificial intelligence approaches (computational tools such as deep learning and neuronal networks) are now reaching atomistic structural levels and temporal resolutions relevant to cell phenomena. Additionally, a new dimension of FRET has been opened with hybrid/integrative modeling, where bio-macromolecular systems are studied simultaneously through a combination of experimental techniques (such as small-angle neutron and small-angle X-ray scatterings, along with NMR, EPR, and FRET spectroscopies), as reviewed in [115]. Single-molecule fluorescence spectroscopy is an emerging field in which FRET is a necessary partner, as demonstrated in a recent study characterizing the coexistence of stable oligomers of amyloid- β 42 within a heterogeneous and dynamic sample [116].

Author Contributions: Conceptualization, F.J.B. and S.S.A.; writing, S.S.A. and F.J.B.; illustrations, S.S.A.; review and editing, F.J.B. All authors have read and agreed to the published version of the manuscript.

Funding: The research work quoted in this review was supported by multiple grants from the National Council for Research and Technology of Argentina (CONICET) and the Ministry of Science, Technology and Innovative Production of Argentina (Mincyt) to F.J.B. and from ANPIDTYI (PICT 2019-02687) and Universidad Nacional del Sur (PGI 24/B282) to S.S.A.

Institutional Review Board Statement: Not applicable.

Informed Consent Statement: Not applicable.

Data Availability Statement: Not applicable.

Conflicts of Interest: The authors declare no conflicts of interest.

References

1. Singer, A.S.J.; Nicolson, G.L. The Fluid Mosaic Model of the Structure of Cell Membranes. *Science* **1972**, *175*, 720–731. [[CrossRef](#)]
2. Engelman, D.M. Membranes are more mosaic than fluid. *Nature* **2005**, *438*, 578–580. [[CrossRef](#)]
3. Bagatolli, L.A. Microscopy imaging of membrane domains. *Biochim. Biophys. Acta* **2010**, *1798*, 1285. [[CrossRef](#)]
4. Goñi, F.M. The basic structure and dynamics of cell membranes: An update of the Singer-Nicolson model. *Biochim. Biophys. Acta* **2014**, *1838*, 1467–1476. [[CrossRef](#)]
5. Nicolson, G.L. The fluid-mosaic model of membrane structure: Still relevant to understanding the structure, function and dynamics of biological membranes after more than 40 years. *Biochim. Biophys. Acta* **2014**, *1838*, 1451–1466. [[CrossRef](#)] [[PubMed](#)]
6. Tweet, A.G.; Bellamy, W.D.; Gaines, G.L. Fluorescence quenching and energy transfer in monomolecular films containing chlorophyll. *J. Chem. Phys.* **1964**, *41*, 2068. [[CrossRef](#)]
7. Vanderkooi, J.M.; Ierokomas, A.; Nakamura, H.; Martonosi, A. Fluorescence energy transfer between Ca²⁺ transport ATPase molecules in artificial membranes. *Biochemistry* **1977**, *16*, 1262–1267. [[CrossRef](#)] [[PubMed](#)]
8. Veatch, W.; Stryer, L. The dimeric nature of the Gramicidin A transmembrane channel: Conductance and fluorescence energy transfer studies of hybrid channels. *J. Mol. Biol.* **1977**, *113*, 89–102. [[CrossRef](#)] [[PubMed](#)]
9. Cantley, L.C.; Hammes, G.G. Investigation of quercetin binding sites on chloroplast coupling factor 1. *Biochemistry* **1976**, *15*, 1–8. [[CrossRef](#)] [[PubMed](#)]
10. Shaklai, N.; Yguerabide, J.; Ranney, H.M. Interaction of hemoglobin with red blood cell membranes as shown by a fluorescent chromophore. *Biochemistry* **1977**, *16*, 5585–5592. [[CrossRef](#)] [[PubMed](#)]
11. Shaklai, N.; Yguerabide, J.; Ranney, H.M. Classification and location of hemoglobin binding sites on red blood cell membranes. *Biochemistry* **1977**, *16*, 5593–5597. [[CrossRef](#)]
12. Fung, B.K.-K.; Stryer, L. Surface density determination in membranes by fluorescence energy transfer. *Biochemistry* **1978**, *17*, 5241–5248. [[CrossRef](#)] [[PubMed](#)]
13. Baird, B.; Pick, U.; Hammes, G.G. Structural investigation of reconstituted chloroplast ATPase with fluorescence measurements. *J. Bio. Chem.* **1979**, *254*, 3818–3825. [[CrossRef](#)]
14. Fleming, P.J.; Koppel, D.E.; Lau, A.L.Y.; Strittmatter, P. Intramembrane position of the fluorescent tryptophanyl residue in the membrane-bound cytochrome b₅. *Biochemistry* **1979**, *18*, 5458–5464. [[CrossRef](#)] [[PubMed](#)]
15. Koppel, D.E.; Fleming, P.J.; Strittmatter, P. Intramembrane positions of membrane-bound chromophores determined by excitation energy transfer. *Biochemistry* **1979**, *18*, 5450–5457. [[CrossRef](#)] [[PubMed](#)]
16. Sklar, L.A.; Doody, M.C.; Gotto, A.M.; Pownall, H.J. Serum lipoprotein structure: Resonance energy transfer localization of fluorescent probes. *Biochemistry* **1980**, *19*, 1294–1301. [[CrossRef](#)] [[PubMed](#)]
17. Gutiérrez-Merino, C. Quantitation of the Forster energy transfer for two-dimensional systems. I. Lateral phase separation in unilamellar vesicles formed by binary phospholipid mixtures. *Biophys. Chem.* **1981**, *14*, 247–257.
18. Gutiérrez-Merino, C. Quantitation of the Forster energy transfer for two-dimensional systems. II. Protein distribution and aggregation state in biological membranes. *Biophys. Chem.* **1981**, *14*, 259–266. [[CrossRef](#)]
19. Snyder, B.; Freire, E. Fluorescence energy transfer in two dimensions. A numeric solution for random and nonrandom distributions. *Biophys. J.* **1982**, *40*, 137–148. [[CrossRef](#)]
20. Eisinger, J.; Flores, J. The relative locations of intramembrane fluorescent probes and the cytosol hemoglobin in erythrocytes, studied by transverse resonance energy transfer. *Biophys. J.* **1982**, *37*, 6–7. [[CrossRef](#)]
21. Doody, M.C.; Skalar, L.A.; Pownall, H.J.; Sparrow, J.T.; Gotto, A.M.; Smith, L.C. A simplified approach to resonance energy transfer in membranes, lipoproteins, and spatially restricted systems. *Biophys. Chem.* **1983**, *17*, 139–152. [[CrossRef](#)]
22. Holowka, D.; Baird, B. Structural studies on the membrane-bound immunoglobulin E-receptor complex 1. Characterization of large plasma membrane vesicles from rat basophilic leukemia cells and insertion of amphipathic fluorescent probes. *Biochemistry* **1983**, *22*, 3466–3474. [[CrossRef](#)]
23. Holowka, D.; Baird, B. Structural studies on the membrane-bound immunoglobulin E-receptor complex 2. Mapping the distance between sites on IgE and the membrane surface. *Biochemistry* **1983**, *22*, 3475–3484. [[CrossRef](#)]
24. Isaacs, B.S.; Husten, E.J.; Esmon, C.T.; Johnson, A.E. A domain of membrane-bound coagulation factor Va is located far from the phospholipid surface. A fluorescence energy transfer measurement. *Biochemistry* **1986**, *25*, 4958–4969. [[CrossRef](#)] [[PubMed](#)]

25. Gryczynski, I.; Wiczak, W.; Johnson, M.L.; Cheung, H.C.; Wang, C.K.; Lakowicz, J.R. Resolution of end-to-end distance distributions of flexible molecules using quenching-induced variations of the Forster distance for fluorescence energy transfer. *Biophys. J.* **1988**, *54*, 577–586. [[CrossRef](#)]
26. Lakowicz, J.R.; Gryczynski, I.; Cheung, H.C.; Wang, C.-K.; Johnson, M.L.; Joshi, N. Distance distributions in proteins recovered by using frequency-domain fluorometry. Applications to troponin I and its complex with troponin C. *Biochemistry* **1988**, *27*, 9149–9160. [[CrossRef](#)]
27. Trauble, H.; Sackmann, E. Studies of the crystalline-liquid crystalline phase transition of lipid model membranes. 3. Structure of a steroid-lecithin system below and above the lipid-phase transition. *J. Am. Chem. Soc.* **1972**, *94*, 4499–4510. [[CrossRef](#)]
28. Förster, T. Intermolecular energy migration and fluorescence. *Ann. Phys.* **1948**, *2*, 55–75. [[CrossRef](#)]
29. Gutiérrez-Merino, C.; Munkonge, F.; Mata, A.M.; East, J.M.; Levinson, B.L.; Napier, R.M.; Lee, A.G. The position of the ATP binding site on the (Ca²⁺ + Mg²⁺)-ATPase. *Biochim. Biophys. Acta* **1987**, *897*, 207–216. [[CrossRef](#)] [[PubMed](#)]
30. Cuenda, A.; Henao, F.; Gutiérrez-Merino, C. Distances between functional sites of the Ca²⁺ + Mg²⁺-ATPase from sarcoplasmic reticulum using Co²⁺ as a spectroscopic ruler. *Eur. J. Biochem.* **1990**, *194*, 663–670. [[CrossRef](#)]
31. Centeno, F.; Gutiérrez-Merino, C. Location of functional centers in the microsomal cytochrome P450 system. *Biochemistry* **1992**, *31*, 8473–8481. [[CrossRef](#)]
32. Gutiérrez-Merino, C.; Centeno, F.; Garcia-Martin, E.; Merino, J.M. Fluorescence energy transfer as a tool to locate functional sites in membrane proteins. *Biochem. Soc. Trans.* **1994**, *22*, 784–788. [[CrossRef](#)]
33. Gutiérrez-Merino, C.; Molina, A.; Escudero, B.; Diez, A.; Laynez, J. Interaction of the Local Anesthetics Dibucaine and Tetracaine with Sarcoplasmic Reticulum Membranes. Differential Scanning Calorimetry and Fluorescence Studies. *Biochemistry* **1989**, *28*, 3398–3406. [[CrossRef](#)]
34. Barrantes, F.J. Structure and function meet at the nicotinic acetylcholine receptor-lipid interface. *Pharmacol. Res.* **2023**, *190*, 106729. [[CrossRef](#)]
35. Karlin, A.; Akabas, M.H. Toward a structural basis for the function of nicotinic acetylcholine receptors and their cousins. *Neuron* **1995**, *6*, 1231–1244. [[CrossRef](#)]
36. Le Novère, N.; Changeux, J.P. Molecular evolution of the nicotinic acetylcholine receptor: An example of multigene family in excitable cells. *J. Mol. Evol.* **1995**, *40*, 155–172. [[CrossRef](#)]
37. Changeux, J.P.; Edelman, S.J. Allosteric receptors after 30 years. *Neuron* **1998**, *5*, 959–980. [[CrossRef](#)]
38. Paterson, D.; Nordberg, A. Neuronal nicotinic receptors in the human brain. *Prog. Neurobiol.* **2000**, *61*, 75–111. [[CrossRef](#)] [[PubMed](#)]
39. Unwin, N. Refined structure of the nicotinic acetylcholine receptor at 4 Å resolution. *J. Mol. Biol.* **2005**, *346*, 967–989. [[CrossRef](#)] [[PubMed](#)]
40. Baenziger, J.E.; Corringer, P.J. 3D structure and allosteric modulation of the transmembrane domain of pentameric ligand-gated ion channels. *Neuropharmacology* **2011**, *60*, 116–125. [[CrossRef](#)] [[PubMed](#)]
41. Baenziger, J.E.; daCosta, C.J.B. Molecular mechanisms of acetylcholine receptor-lipid interactions: From model membranes to human biology. *Biophys. Rev.* **2013**, *5*, 1–9. [[CrossRef](#)]
42. Corradi, J.; Bouzat, C. Understanding the bases of function and modulation of $\alpha 7$ nicotinic receptors: Implications for drug discovery. *Mol. Pharmacol.* **2016**, *90*, 288–299. [[CrossRef](#)]
43. Zarkadas, E.; Pebay-Peyroula, E.; Thompson, M.J.; Schoehn, G.; Uchański, T.; Steyaert, J.; Chipot, C.; Dehez, F.; Baenziger, J.E.; Nury, H. Conformational transitions and ligand-binding to a muscle-type nicotinic acetylcholine receptor. *Neuron* **2020**, *110*, 1358–1370. [[CrossRef](#)] [[PubMed](#)]
44. Absalom, N.L.; Schofield, P.R.; Lewis, T.M. Pore structure of the Cys-loop ligand gated ion channels. *Neurochem. Res.* **2009**, *34*, 1805–1815. [[CrossRef](#)] [[PubMed](#)]
45. Morales-Pérez, C.L.; Noviello, C.M.; Hibbs, R.E. X-ray structure of the human $\alpha 4\beta 2$ nicotinic receptor. *Nature* **2016**, *538*, 411–415. [[CrossRef](#)] [[PubMed](#)]
46. Rahman, M.M.; Basta, T.; Teng, J.; Lee, M.; Worrell, B.T.; Stowell, M.H.B.; Hibbs, R.E. Structural mechanism of muscle nicotinic receptor desensitization and block by curare. *Nat. Struct. Mol. Biol.* **2022**, *29*, 386–394. [[CrossRef](#)]
47. daCosta, C.J.B.; Wagg, I.D.; McKay, M.E.; Baenziger, J.E. Phosphatidic acid and phosphatidylserine have distinct structural and functional interactions with the nicotinic acetylcholine receptor. *J. Biol. Chem.* **2004**, *279*, 14967–14974. [[CrossRef](#)]
48. Pediconi, M.F.; Gallegos, C.E.; Barrantes, F.J. Metabolic cholesterol depletion hinders cell-surface trafficking of the nicotinic acetylcholine receptor. *Neuroscience* **2004**, *128*, 239–249. [[CrossRef](#)]
49. Baier, C.J.; Barrantes, F.J. Sphingolipids are necessary for nicotinic acetylcholine receptor export in the early secretory pathway. *J. Neurochem.* **2007**, *101*, 1072–1084. [[CrossRef](#)]
50. Baenziger, J.E.; Hénault, C.M.; Therien, J.P.D.; Sun, J. Nicotinic acetylcholine receptor-lipid interactions: Mechanistic insight and biological function. *Biochim. Biophys. Acta Biomembr.* **2015**, *1848*, 1806–1817. [[CrossRef](#)] [[PubMed](#)]
51. Marsh, D.; Barrantes, F.J. Immobilized lipid in acetylcholine receptor-rich membranes from *Torpedo marmorata*. *Proc. Natl. Acad. Sci. USA* **1978**, *75*, 4329–4333. [[CrossRef](#)]
52. Antollini, S.S.; Soto, M.A.; Bonini de Romanelli, I.; Gutiérrez-Merino, C.; Sotomayor, P.; Barrantes, F.J. Physical state of bulk and protein associated lipid in nicotinic acetylcholine receptor-rich membrane studied by Laurdan generalized polarization and fluorescence energy transfer. *Biophys. J.* **1996**, *70*, 1275–1284. [[CrossRef](#)] [[PubMed](#)]

53. Fernández Nuevas, G.A.; Barrantes, F.J.; Antollini, S.S. Conformation-sensitive steroid and fatty acid sites in the transmembrane domain of the nicotinic acetylcholine receptor. *Biochemistry* **2007**, *46*, 3503–3512. [[CrossRef](#)]
54. Lee, A.G. Lipid-protein interactions in biological membranes: A structural perspective. *Biochim. Biophys. Acta* **2003**, *1612*, 1–40. [[CrossRef](#)] [[PubMed](#)]
55. Bechara, C.; Robinson, C.V. Different modes of lipid binding to membrane proteins probed by mass spectrometry. *J. Am. Chem. Soc.* **2015**, *137*, 5240–5247. [[CrossRef](#)] [[PubMed](#)]
56. Landreh, M.; Marty, M.T.; Gault, J.; Robinson, C.V. A sliding selectivity scale for lipid binding to membrane proteins. *Curr. Opin. Struct. Biol.* **2016**, *39*, 54–60. [[CrossRef](#)]
57. Bolla, J.R.; Corey, R.A.; Sahin, C.; Gault, J.; Hummer, A.; Hopper, J.T.S.; Lane, D.P.; Drew, D.; Allison, T.M.; Stansfeld, P.J.; et al. A mass spectrometry-based approach to distinguish annular and specific lipid binding to membrane proteins. *Angew. Chem. Int. Ed. Engl.* **2020**, *59*, 3523–3528. [[CrossRef](#)]
58. Schaaf, C.P. Nicotinic acetylcholine receptors in human genetic disease. *Genet. Med.* **2014**, *16*, 649–656. [[CrossRef](#)]
59. Yadav, R.S.; Tiwari, N.K. Lipid integration in neurodegeneration: An overview of Alzheimer's disease. *Mol. Neurobiol.* **2014**, *50*, 168–176. [[CrossRef](#)]
60. Op den Kamp, J.A.F. Lipid asymmetry in membranes. *Annu. Rev. Biochem.* **1979**, *48*, 47–71. [[CrossRef](#)]
61. Devaux, P.F. Static and dynamic lipid asymmetry in cell membranes. *Biochemistry* **1991**, *30*, 1163–1173. [[CrossRef](#)]
62. Schroeder, F. *Methods for Studying Membrane Fluidity*; Alan, R., Ed.; Liss Inc.: New York, NY, USA, 1988; pp. 193–217.
63. Wood, W.G.; Gorka, C.; Schroeder, F. Acute and chronic effects of ethanol on transbilayer membrane domains. *J. Neurochem.* **1989**, *52*, 1925–1930. [[CrossRef](#)] [[PubMed](#)]
64. Wood, W.G.; Schroeder, F.; Hogy, L.; Rao, A.M.; Nemezc, G. Asymmetric distribution of a fluorescent sterol in synaptic plasma membranes: Effects of chronic ethanol consumption. *Biochim. Biophys. Acta* **1990**, *1025*, 243–246. [[CrossRef](#)] [[PubMed](#)]
65. Jain, M.K.; Wagner, R.C. *Introduction to Biological Membranes*; John Wiley and Sons: New York, NY, USA, 1980; p. 382.
66. Herbette, L.; DeFoor, P.; Fleischer, S.; Pascolini, D.; Scarpa, A.; Blasie, J.K. The separate profile structures of the functional calcium pump protein and the phospholipid bilayer within isolated sarcoplasmic reticulum membranes determined by X-ray and neutron diffraction. *Biochim. Biophys. Acta* **1985**, *817*, 103–122. [[CrossRef](#)] [[PubMed](#)]
67. Gutiérrez-Merino, C.; Pietrasanta, L.; Bonini de Romanelli, I.; Barrantes, F.J. Preferential distribution of fluorescent phospholipid probes NBD-phosphatidylcholine and Rhodamine-phosphatidylethanolamine in the exofacial leaflet of acetylcholine receptor-rich membranes from *Torpedo marmorata*. *Biochemistry* **1995**, *34*, 4846–4855. [[CrossRef](#)] [[PubMed](#)]
68. Scher, M.G.; Bloch, R.J. Phospholipid asymmetry in acetylcholine receptor clusters. *Exp. Cell Res.* **1993**, *208*, 485–491. [[CrossRef](#)] [[PubMed](#)]
69. González-Ros, J.M.; Llanillo, M.; Paraschos, A.; Martínez-Carrion, M. Lipid environment of acetylcholine receptor from *Torpedo californica*. *Biochemistry* **1982**, *21*, 3467–3474. [[CrossRef](#)] [[PubMed](#)]
70. Rotstein, N.P.; Arias, H.R.; Barrantes, F.J.; Aveldaño, M.I. Composition of lipids in elasmobranch electric organ and acetylcholine receptor membranes. *J. Neurochem.* **1987**, *49*, 1333–1340. [[CrossRef](#)]
71. Narayanaswami, V.; McNamee, M.G. Protein-lipid interactions and *Torpedo californica* nicotinic acetylcholine receptor function. 2. Membrane fluidity and ligand-mediated alteration in the accessibility of gamma subunit cysteine residues to cholesterol. *Biochemistry* **1993**, *32*, 12420–12427. [[CrossRef](#)]
72. Jansson, C.; Harmala, A.S.; Toivola, D.M.; Slotte, J.P. Effects of the phospholipids environment in the plasma membrane on receptor interaction with the adenylyl cyclase complex of intact cells. *Biochim. Biophys. Acta* **1993**, *1145*, 311–319. [[CrossRef](#)]
73. Ellena, J.F.; Blazing, M.A.; McNamee, M.G. Lipid-protein interactions in reconstituted membranes containing Acetylcholine receptor. *Biochemistry* **1983**, *22*, 5523–5535. [[CrossRef](#)]
74. Marsh, D.; Watts, A.; Barrantes, F.J. Phospholipid chain immobilization and steroid rotational immobilization in acetylcholine receptor-rich membranes from *Torpedo marmorata*. *Biochim. Biophys. Acta* **1981**, *645*, 97–101. [[CrossRef](#)]
75. Bonini, I.C.; Antollini, S.S.; Gutiérrez-Merino, C.; Barrantes, F.J. Sphingomyelin composition and physical asymmetries in native acetylcholine receptor-rich membranes. *Eur. Biophys. J.* **2002**, *31*, 417–427. [[CrossRef](#)]
76. Parasassi, T.; Conti, F.; Gratton, E. Time-resolved fluorescence emission spectra of laurdan in phospholipid vesicles by multifrequency phase and modulation fluorometry. *Cell. Mol. Biol.* **1986**, *32*, 103–108.
77. Parasassi, T.; De Stasio, G.; d'Ubaldo, A.; Gratton, E. Phase fluctuation in phospholipid membranes revealed by laurdan fluorescence. *Biophys. J.* **1990**, *57*, 1179–1186. [[CrossRef](#)] [[PubMed](#)]
78. Parasassi, T.; De Stasio, G.; Ravagnan, G.; Rusch, R.; Gratton, E. Quantitation of lipid phases in phospholipid vesicles by the GP of laurdan fluorescence. *Biophys. J.* **1991**, *60*, 179–189. [[CrossRef](#)] [[PubMed](#)]
79. Gunther, G.; Malacrida, L.; Jameson, D.M.; Gratton, E.; Sánchez, S.A. LAURDAN since Weber: The Quest for Visualizing Membrane Heterogeneity. *Acc. Chem. Res.* **2021**, *54*, 976–987. [[CrossRef](#)] [[PubMed](#)]
80. Chong, P.L.-G. Effect of hydrostatic pressure on the location of PRODAN in lipid bilayers and cellular membranes. *Biochemistry* **1988**, *27*, 399–404. [[CrossRef](#)] [[PubMed](#)]
81. Chong, P.L.-G. Interactions of PRODAN and laurdan with membranes at high pressure. *High Press. Res.* **1990**, *5*, 761–763. [[CrossRef](#)]
82. Unwin, N. Structure and action of the nicotinic acetylcholine receptor explored by electron microscopy. *FEBS Lett.* **2003**, *555*, 91–95. [[CrossRef](#)] [[PubMed](#)]

83. Rand, R.T. Interacting phospholipid bilayer: Measured forces and induced structural changes. *Annu. Rev. Biophys. Bioenerg.* **1981**, *10*, 277–314. [[CrossRef](#)]
84. Antollini, S.S.; Barrantes, F.J. Unique effects of different fatty acid species on the physical properties of the torpedo acetylcholine receptor membrane. *J. Biol. Chem.* **2002**, *277*, 1249–1254. [[CrossRef](#)] [[PubMed](#)]
85. Bermúdez, V.; Antollini, S.S.; Nievas, G.A.F.; Aveldaño, M.I.; Barrantes, F.J. Partition profile of the nicotinic acetylcholine receptor in lipid domains upon reconstitution. *J. Lipid Res.* **2010**, *51*, 2629–2641. [[CrossRef](#)]
86. Perillo, V.L.; Peñalva, D.A.; Vitale, A.J.; Barrantes, F.J.; Antollini, S.S. Transbilayer asymmetry and sphingomyelin composition modulate the preferential membrane partitioning of the nicotinic acetylcholine receptor in Lo domains. *Arch. Biochem. Biophys.* **2016**, *591*, 76–86. [[CrossRef](#)] [[PubMed](#)]
87. Franklin, J.L. Redox regulation of the intrinsic pathway in neuronal apoptosis. *Antioxid. Redox Signal.* **2011**, *14*, 1437–1448. [[CrossRef](#)]
88. Dhapola, R.; Beura, S.K.; Sharma, P.; Singh, S.K.; HariKrishnaReddy, D. Oxidative stress in Alzheimer’s disease: Current knowledge of signaling pathways and therapeutics. *Mol. Biol. Rep.* **2024**, *51*, 48. [[CrossRef](#)]
89. Eide, L.; McMurray, C.T. Culture of adult mouse neurons. *BioTechniques* **2005**, *38*, 99–104. [[CrossRef](#)] [[PubMed](#)]
90. Schild, D.; Geiling, H.; Bischofberger, J. Imaging of L-type Ca^{2+} channels in olfactory bulb neurones using fluorescent dihydropyridine and a styryl dye. *J. Neurosci. Methods* **1995**, *59*, 183–190. [[CrossRef](#)]
91. McKinney, R.A. Physiological roles of spinemotility: Development plasticity and disorders. *Biochem. Soc. Trans.* **2005**, *33*, 1299–1302. [[CrossRef](#)]
92. Samhan-Arias, A.K.; García-Bereguiaín, M.A.; Martín-Romero, F.J.; Gutiérrez-Merino, C. Regionalization of plasma membrane-bound flavoproteins of cerebellar granule neurons in culture by fluorescence energy transfer imaging. *J. Fluoresc.* **2006**, *16*, 393–401. [[CrossRef](#)]
93. Villalba, J.M.; Navarro, F.; Gómez-Díaz, C.; Arroyo, A.; Bello, R.I.; Navas, P. Role of cytochrome b_5 reductase on the antioxidant function of coenzyme Q in the plasma membrane. *Mol. Asp. Med.* **1997**, *18* (Suppl. S1), S7–S13. [[CrossRef](#)] [[PubMed](#)]
94. Chatenay-Rivauday, C.; Cakar, Z.P.; Jenö, P.; Kuzmenko, E.S.; Fiedler, K. Caveolae: Biochemical analysis. *Mol. Biol. Rep.* **2004**, *31*, 67–84. [[CrossRef](#)] [[PubMed](#)]
95. Samhan-Arias, A.K.; Garcia-Bereguiaín, M.A.; Martin-Romero, F.J.; Gutiérrez-Merino, C. Clustering of plasma membrane-bound cytochrome b_5 reductase within ‘lipid raft’ microdomains of the neuronal plasma membrane. *Mol. Cell. Neurosci.* **2009**, *40*, 14–26. [[CrossRef](#)] [[PubMed](#)]
96. Samhan-Arias, A.K.; López-Sánchez, C.; Marques-da-Silva, D.; Lagoa, R.; Garcia-Lopez, V.; García-Martínez, V.; Gutiérrez-Merino, C. High expression of cytochrome b 5 reductase isoform 3/cytochrome b 5 system in the cerebellum and pyramidal neurons of adult rat brain. *Brain Struct. Funct.* **2015**, *221*, 2147–2162. [[CrossRef](#)] [[PubMed](#)]
97. Marques-da-Silva, D.; Samhan-Arias, A.K.; Tiago, T.; Gutiérrez-Merino, C. L-type calcium channels and cytochrome b_5 reductase are components of protein complexes tightly associated with lipid rafts microdomains of the neuronal plasma membrane. *J. Proteom.* **2010**, *73*, 1502–1510. [[CrossRef](#)] [[PubMed](#)]
98. Samhan-Arias, A.K.; Marques-da-Silva, D.; Yanamala, N.; Gutiérrez-Merino, C. Stimulation and clustering of cytochrome b_5 reductase in caveolin-rich lipid microdomains is an early event in oxidative stress-mediated apoptosis of cerebellar granule neurons. *J. Proteom.* **2012**, *75*, 2934–2949. [[CrossRef](#)]
99. Marques-da-Silva, D.; Gutiérrez-Merino, C. L-type voltage-operated calcium channels, N-methyl-D-aspartate receptors and neuronal nitric-oxide synthase form a calcium/redox nano-transducer within lipid rafts. *Biochem. Biophys. Res. Commun.* **2012**, *420*, 257–262. [[CrossRef](#)]
100. Marques-da-Silva, D.; Gutiérrez-Merino, C. Caveolin-rich lipid rafts of the plasma membrane of mature cerebellar granule neurons are microcompartments for calcium/reactive oxygen and nitrogen species cross-talk signaling. *Cell Calcium* **2014**, *56*, 108–123. [[CrossRef](#)]
101. Poejo, J.; Salazar, J.; Mata, A.M.; Gutiérrez-Merino, C. Binding of Amyloid- β (1–42)-Calmodulin Complexes to Plasma Membrane Lipid Rafts in Cerebellar Granule Neurons Alters Resting Cytosolic Calcium Homeostasis. *Int. J. Mol. Sci.* **2021**, *22*, 1984. [[CrossRef](#)]
102. Poejo, J.; Orantos-Aguilera, Y.; Martin-Romero, F.J.; Mata, A.M.; Gutiérrez-Merino, C. Internalized Amyloid- β (1–42) Peptide inhibits the store-operated calcium entry in HT-22 cells. *Int. J. Mol. Sci.* **2022**, *23*, 12678. [[CrossRef](#)]
103. Salazar, J.; Samhan-Arias, A.K.; Gutiérrez-Merino, C. Hexa-histidine, a peptide with versatile applications in the study of Amyloid- β (1–42) molecular mechanisms of action. *Molecules* **2023**, *28*, 7138. [[CrossRef](#)]
104. Förster, T. Experimentelle und theoretische Untersuchung des zwischenmolekularen Übergangs von Elektronenanregungsenergie. *Zeitschr. Naturforschung A* **1949**, *4*, 321–327. [[CrossRef](#)]
105. Stryer, L.; Haugland, R.P. Energy Transfer: A Spectroscopic Ruler. *Proc. Natl. Acad. Sci. USA* **1967**, *58*, 719–726. [[CrossRef](#)] [[PubMed](#)]
106. Weber, G.; Farris, F. Synthesis and spectral properties of a hydrophobic fluorescent probe: 6-propionyl-2-(dimethylamino)naphthalene. *Biochemistry* **1979**, *18*, 3075–3078. [[CrossRef](#)]
107. Hoppe, A.D.; Shorte, S.L.; Swanson, J.A.; Heintzmann, R. Three-dimensional FRET reconstruction microscopy for analysis of dynamic molecular interactions in live cells. *Biophys. J.* **2008**, *95*, 400–418. [[CrossRef](#)]

108. Ágnes, S.; Tímea, S.-S.; János, S.; Peter, N. Quo vadis FRET? Förster's method in the era of superresolution. *Methods Appl. Fluoresc.* **2020**, *8*, 032003.
109. Trumpp, M.; Oliveras, A.; Gonschior, H.; Ast, J.; Hodson, D.J.; Knaus, P.; Lehmann, M.; Birol, M.; Broichhagen, J. Enzyme self-label-bound ATTO700 in single-molecule and super-resolution microscopy. *Chem. Commun.* **2022**, *58*, 13724–13727. [[CrossRef](#)] [[PubMed](#)]
110. Tsien, R.Y.; Miyawaki, A. Seeing the machinery of live cells. *Science* **1998**, *280*, 1954–1955. [[CrossRef](#)]
111. Szalai, A.M.; Zaza, C.; Stefani, F.D. Super-resolution FRET measurements. *Nanoscale* **2021**, *13*, 18421–18433. [[CrossRef](#)] [[PubMed](#)]
112. Smith, J.T.; Sinsuebphon, N.; Rudkouskaya, A.; Michalet, X.; Intes, X.; Barroso, M. In vivo quantitative FRET small animal imaging: Intensity versus lifetime-based FRET. *Biophys. Rep.* **2023**, *3*, 100110. [[CrossRef](#)]
113. Carro, A.C.; Piccini, L.E.; Damonte, E.B. Blockade of dengue virus entry into myeloid cells by endocytic inhibitors in the presence or absence of antibodies. *PLoS. Negl. Trop. Dis.* **2018**, *12*, e0006685. [[CrossRef](#)] [[PubMed](#)]
114. Deng, S.; Chen, J.; Gao, Z.; Fan, C.; Yan, Q.; Wang, Y. Effects of donor and acceptor's fluorescence lifetimes on the method of applying Förster resonance energy transfer in STED microscopy. *J. Microsc.* **2018**, *269*, 59–65. [[CrossRef](#)]
115. Dimura, M.; Peulen, T.O.; Hanke, C.A.; Prakash, A.; Gohlke, H.; Seidel, C.A. Quantitative FRET studies and integrative modeling unravel the structure and dynamics of biomolecular systems. *Curr. Opin. Struct. Biol.* **2016**, *40*, 163–185. [[CrossRef](#)] [[PubMed](#)]
116. Meng, F.; Kim, J.-Y.; Gopich, I.V.; Chung, H.S. Single-molecule FRET and molecular diffusion analysis characterize stable oligomers of Amyloid- β 42 of extremely low population. *PNAS Nexus* **2023**, *2*, pgad253. [[CrossRef](#)] [[PubMed](#)]

Disclaimer/Publisher's Note: The statements, opinions and data contained in all publications are solely those of the individual author(s) and contributor(s) and not of MDPI and/or the editor(s). MDPI and/or the editor(s) disclaim responsibility for any injury to people or property resulting from any ideas, methods, instructions or products referred to in the content.